

***p-n* Junction Rectifying Characteristics of Purely *n*-Type GaN-Based Structures**P. Zuo,¹ Y. Jiang,¹ Z. G. Ma,¹ L. Wang,¹ B. Zhao,¹ Y. F. Li,¹ G. Yue,¹ H. Y. Wu,¹ H. J. Yan,¹ H. Q. Jia,¹ W. X. Wang,¹ J. M. Zhou,¹ Q. Sun,² W. M. Liu,³ An-Chun Ji,^{2,*} and H. Chen^{1,†}¹*Key Laboratory for Renewable Energy, Beijing Key Laboratory for New Energy Materials and Devices, Beijing National Laboratory for Condensed Matter Physics, Institute of Physics, Chinese Academy of Sciences, Beijing 100190, China*²*Department of Physics, Capital Normal University, Beijing 100048, China*³*Laboratory of Condensed Matter Theory and Materials Computation, Institute of Physics, Chinese Academy of Sciences, Beijing 100190, China*

(Received 7 August 2016; revised manuscript received 5 June 2017; published 9 August 2017)

The GaN-based *p-n* junction rectifications are important in the development of high-power electronics. Here, we demonstrate that *p-n* junction rectifying characteristics can be realized with pure *n*-type structures by inserting an (In,Ga)N quantum well into the GaN/(Al,Ga)N/GaN double heterostructures. Unlike the usual barriers, the insertion of an (In,Ga)N quantum well, which has an opposite polarization field to that of the (Al,Ga)N barrier, tailors significantly the energy bands of the system. The lifted energy level of the GaN spacer and the formation of the (In,Ga)N/GaN interface barrier can improve the reverse threshold voltage and reduce the forward threshold voltage simultaneously, forming the *p-n* junction rectifying characteristics.

DOI: 10.1103/PhysRevApplied.8.024005

I. INTRODUCTION

The direct-gap III nitrides offer the most viable approach for application in high-power electronics due to their properties of wide band gap, high breakdown field, high saturated electron drift velocity, and availability of heterojunctions [1–11]. For instance, high-electron-mobility transistors have achieved great success in the field of radio-frequency power technology [12–16]. However, a problem has persisted in GaN-based *p-n* junction rectifying characteristics, which was hindered by low *p*-type doping, poor hole mobility, and a deep acceptor level of *p*-type GaN [17–20]. Although enormous efforts have been made to improve *p*-type GaN [21–24], the realization of *p-n* junction rectifying characteristics remains difficult for GaN-based electronics.

Conventional *p-n* junctions are bipolar, consisting of both *p*- and *n*-type carries. Here, we implement an alternative strategy to achieve the *p-n* junction rectifications with unipolar III nitrides, which are free of *p*-type GaN. Although some early attempts have been made in unipolar heterojunctions, such as lightly doped *n*-(Al,Ga)As/*n*-GaAs [25] and *n*-(In,Ga)As/*n*-InP heterojunctions [26], it was shown that the reverse threshold voltages are very small, and the asymmetry of the threshold voltage is hard to be enhanced in unipolar structures.

In this work, we determine a method to reach the *p-n* junction rectifying characteristics by inserting an (In,Ga)N quantum well into GaN/(Al,Ga)N/GaN double heterostructures (DHs). Quantum wells have never been utilized

to modulate the current rectification, since unlike the usual barriers, they could not block the transmitting electrons under bias voltage in pure *n*-type semiconductor structures. Here, we demonstrate that once the (In,Ga)N quantum well is inserted into the GaN/(Al,Ga)N/GaN DHs, the energy bands are significantly tailored. Because of the giant piezoelectric polarization field in the (In,Ga)N quantum well, which is opposite from that of the (Al,Ga)N barrier, the (In,Ga)N quantum well inclines, lifting the energy level of the GaN spacer and forming the (In,Ga)N/GaN interface barrier. In this case, we find that the forward threshold voltage can be lowered with a large asymmetry of threshold voltage, enabling the realization of *p-n* junction rectifying characteristics in pure *n*-type GaN-based structures.

II. CURRENT-VOLTAGE CHARACTERISTICS OF THE GaN/(Al,Ga)N/GaN DOUBLE HETEROSTRUCTURES

First, GaN/(Al,Ga)N/GaN DHs are grown on sapphire substrates by the metal-organic chemical-vapor-deposition (MOCVD) technique. The sample structures consist of 3- μm *n*-type GaN, 5-nm unintentionally doped (UID) GaN, an $\text{Al}_x\text{Ga}_{1-x}\text{N}$ barrier layer, and a 100-nm *n*-type GaN (see the Appendix). The electron concentration in both *n*-type GaN's is $2 \times 10^{18} \text{ cm}^{-3}$, and the sample is covered by Cr/Ti/Al electrodes with a mesa area of $5000 \mu\text{m}^2$. We fabricate two groups of samples: one has different Al content x of 15% and 25% in 10-nm $\text{Al}_x\text{Ga}_{1-x}\text{N}$, and the other has different thicknesses of 10, 20, and 30 nm for the $\text{Al}_{0.15}\text{Ga}_{0.85}\text{N}$ layers.

* anchun.ji@cnu.edu.cn

† hchen@iphy.ac.cn

Figure 1(a) shows the measured vertical current-voltage characteristics, where the forward and reverse threshold voltages are different. It is quite distinct from the usual semiconductor DHs such as GaAs/(Al, Ga)As/GaAs [28], whose forward and reverse threshold voltages are nearly the same. This is because, due to the giant spontaneous and piezoelectric polarization fields in the (Al,Ga)N barrier, the energy bands of the (Al,Ga)N barrier become inclined; see Fig. 1(b). The polarization fields in the (Al,Ga)N barrier are effectively compensated by +2V forward bias, whereas for -2V reverse bias, a finite residual barrier of the depletion

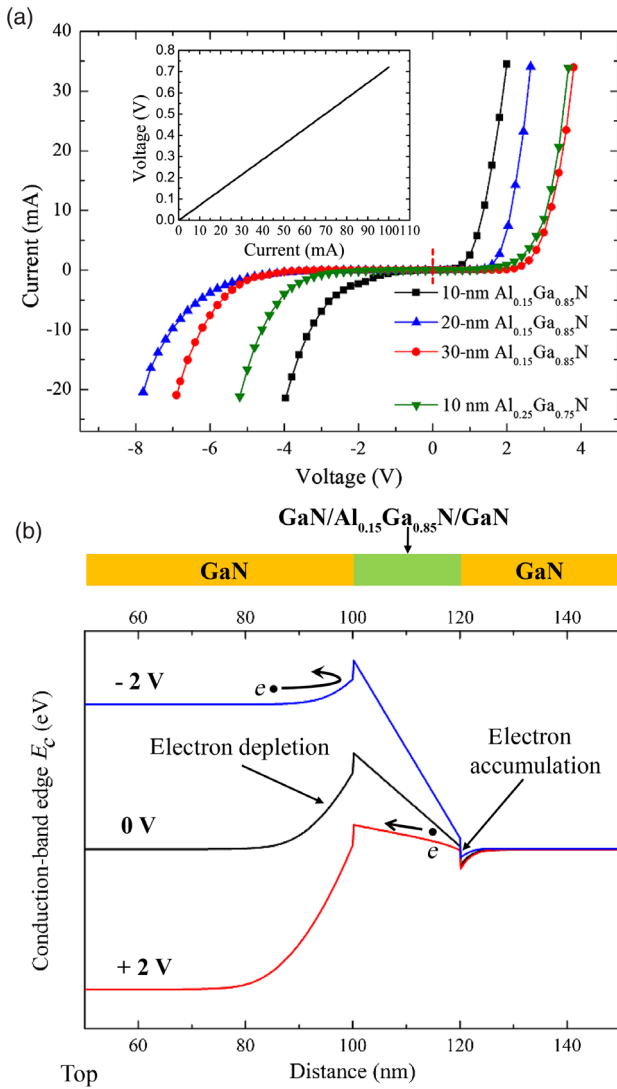


FIG. 1. (a) Vertical I - V relationships of the GaN/ $\text{Al}_x\text{Ga}_{1-x}\text{N}$ /GaN DHs with 10-, 20-, and 30-nm $\text{Al}_{0.15}\text{Ga}_{0.85}\text{N}$, and 10-nm $\text{Al}_{0.25}\text{Ga}_{0.75}\text{N}$, which display weak rectification effects. The positive bias is applied on the top electrode (see the schematic structures of samples in Fig. 6 of the Appendix). The inset shows the Ohmic nature of the contact between the electrode (Cr/Ti/Al) and n -GaN (see the Appendix, Sec. B for details). (b) Conduction-band diagrams of GaN/ $\text{Al}_{0.15}\text{Ga}_{0.85}\text{N}$ /GaN DHs with a 20-nm $\text{Al}_{0.15}\text{Ga}_{0.85}\text{N}$ barrier under different biases [27]. E_c stands for the bottom of the conduction band.

region remains. Thus, a weak rectification effect can be achieved in the GaN/(Al, Ga)N/GaN DHs. However, further improving the rectification ratio is found to be very hard by adjusting the polarization fields of the (Al,Ga)N barrier or inserting an additional (Al,Ga)N barrier into the DHs.

III. CURRENT-VOLTAGE CHARACTERISTICS OF THE (In,Ga)N MODULATED DOUBLE HETEROSTRUCTURES

(In, Ga)N/GaN quantum wells have been extensively studied and applied in optoelectronic devices such as

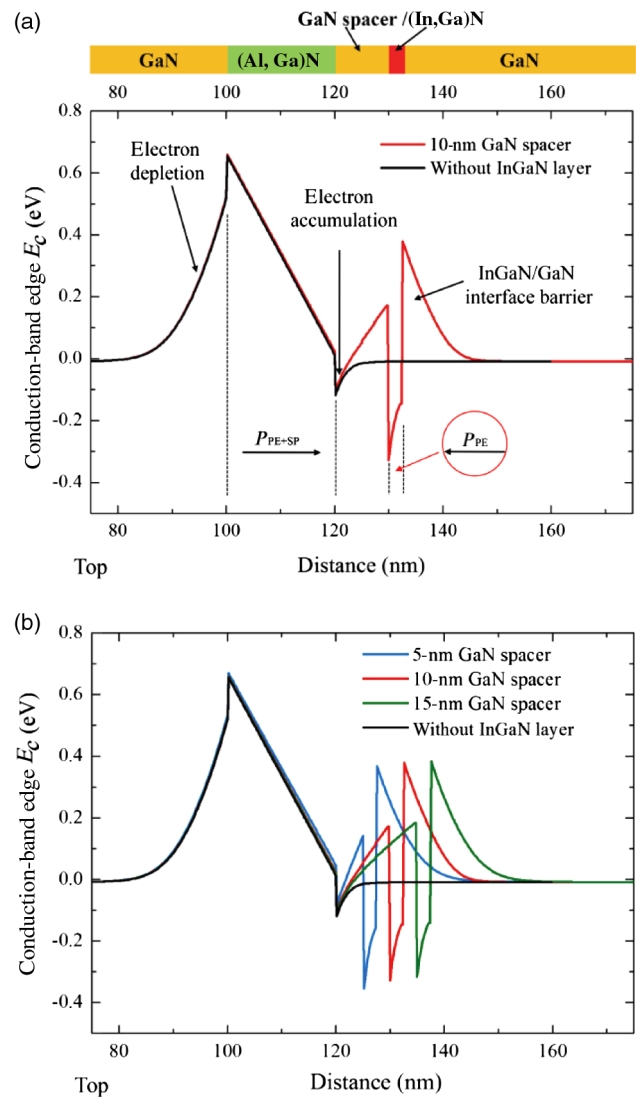


FIG. 2. (a) Conduction-band diagrams of the GaN/ $\text{Al}_{0.15}\text{Ga}_{0.85}\text{N}$ /GaN spacer/ $\text{In}_{0.2}\text{Ga}_{0.8}\text{N}$ /GaN samples with and without the (In,Ga)N layer [27]. The energy-band structures are significantly tailored, exhibiting an (In,Ga)N back barrier and a diffusion barrier between the triangular potential well and (In,Ga)N quantum well. (b) Conduction-band diagrams of the samples with different thicknesses of the GaN spacer.

light-emitting diodes [29–31], lasers [32,33], and solar cells [34,35]. Here, we insert an (In,Ga)N quantum-well layer into GaN/(Al, Ga)N/GaN DHs. The 2.5-nm In_{0.2}Ga_{0.8}N quantum well is grown on the *n*-type GaN, followed by the UID GaN spacer with different thicknesses (5, 10, 15 nm), 20-nm Al_{0.15}Ga_{0.85}N barrier, and 100-nm *n*-type GaN (see the Appendix). Note that the piezoelectric effect in the (In,Ga)N quantum well produces a giant piezoelectric polarization field (P_{PE}), which is opposite from the spontaneous and piezoelectric polarization fields of the (Al,Ga)N layer (P_{SP+PE}) as pictured in Fig. 2(a). The inclined (In,Ga)N quantum well can induce the (In, Ga)N/GaN interface barrier, and the energy level of the GaN spacer becomes bent, induced by spontaneous and piezoelectric polarization in the (Al, Ga)N/GaN heterostructure [36]. This bend results in the accumulation of the electrons in the triangular potential well. Importantly, such modulated energy bands strengthen the restraint of the electrons in the accumulation region with enhanced electron concentration, and they adjust the voltage distribution of the system. Similar energy-band structures for different thicknesses of the GaN spacer are shown in Fig. 2(b).

Figure 3 shows the measured I - V relationships of the (In, Ga)N modulated DHs. Significantly, we observe remarkable rectifying behaviors with small forward threshold voltage and large rectification ratio. The threshold voltages of forward and reverse bias are shown in Table I. In contrast to the case without the (In,Ga)N layer, the sample with the 10-nm GaN spacer presents a smaller forward threshold voltage (+0.9 V), as well as a much larger reverse threshold voltage (−6.7 V). Specifically, a reverse threshold

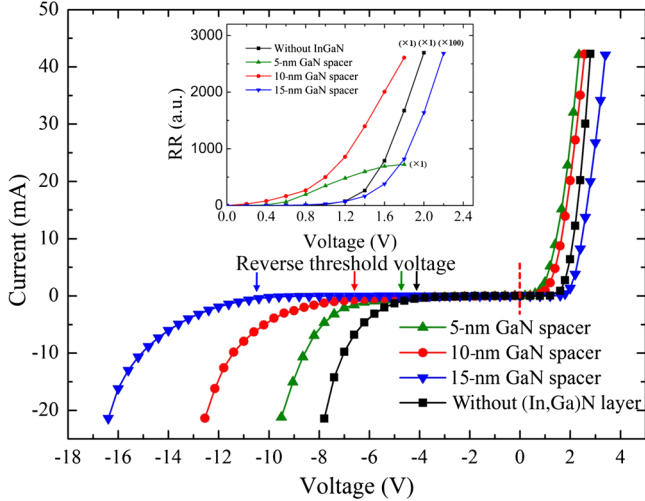


FIG. 3. Measured I - V relationships of the samples with 20-nm Al_{0.15}Ga_{0.85}N and 2.5-nm In_{0.2}Ga_{0.8}N for different thicknesses of the GaN spacer, which display notable rectification effects. Inset: The relationship of the current rectification ratio (RR) and related voltage for the sample without the (In,Ga)N inserting layer, with a 5-, 10-, and 15-nm GaN spacer. Here, the data for the 15-nm GaN spacer should be timed 100 to be the real measurement.

TABLE I. The forward and reverse threshold voltages for the (In,Ga)N modulated samples GaN/Al_{0.15}Ga_{0.85}N/GaN spacer/In_{0.2}Ga_{0.8}N/GaN with different thicknesses of the GaN spacer.

Threshold voltage	Without the (In,Ga)N layer	5-nm GaN spacer	10-nm GaN spacer	15-nm GaN spacer
Forward	1.5 V	0.6 V	0.9 V	1.8 V
Reverse	−4 V	−4.6 V	−6.7 V	−10.6 V

voltage of −10.6 V can be identified for the 15-nm GaN spacer sample, with a high rectification ratio (the rectification ratio is defined as the ratio of forward current to reverse current at a specific applied voltage [37–39]) of 8.2×10^4 at the forward threshold voltage 1.8 V. As such, the (In,Ga)N quantum well plays a significant role in the current rectification in the DHs.

IV. THEORETICAL ANALYSIS OF THE RECTIFYING CHARACTERISTICS

In the thermionic emission [40–42], the current is determined by both the concentration of electrons and the barrier height. First, for zero bias, the current is given by

$$I = \frac{1}{4} n S v_{av} \exp\left(-\frac{qV_b}{kT}\right), \quad (1)$$

where n is the electron concentration, S is the mesa area, $v_{av} = \sqrt{8kT/\pi m^*}$ is the average speed of electrons, and V_b is the barrier height at zero bias.

We take the sample with the 10-nm GaN spacer as an example, with the energy-band structures under different biases as shown in Fig. 4(a). As the voltage V_a is applied on the sample (the positive bias is applied on the top electrode), the energy-band structure changes. For the sample with the (In,Ga)N inserting layer, the voltage drops on the electron depletion region (V_1) and (Al,Ga)N barrier (V_2), as well as on the (In,Ga)N-related region (V_3); see Fig. 4(a). In this case, the barriers encountered by the forward and reverse transporting electrons become $V_+ = V_b - V_2$ for the (Al,Ga)N barrier and $V_- = V_b - |V_1|$ for the barrier of the electron depletion region. The total current $I = I_+ - I_-$ takes the form [42]

$$\begin{aligned} I &= \frac{1}{4} n_+ S v_{av} \exp\left(-\frac{qV_+}{h_+ kT}\right) - \frac{1}{4} n_- S v_{av} \exp\left(-\frac{qV_-}{h_- kT}\right) \\ &= qn_+ \sqrt{\frac{kT}{2\pi m^*}} \exp\left(-\frac{qV_b - qV_2}{h_+ kT}\right) \\ &\quad - qn_- \sqrt{\frac{kT}{2\pi m^*}} \exp\left(-\frac{qV_b + qV_1}{h_- kT}\right), \end{aligned} \quad (2)$$

where n_+ is the electron concentration of the electron accumulation region, n_- is the electron density in *n*-GaN,

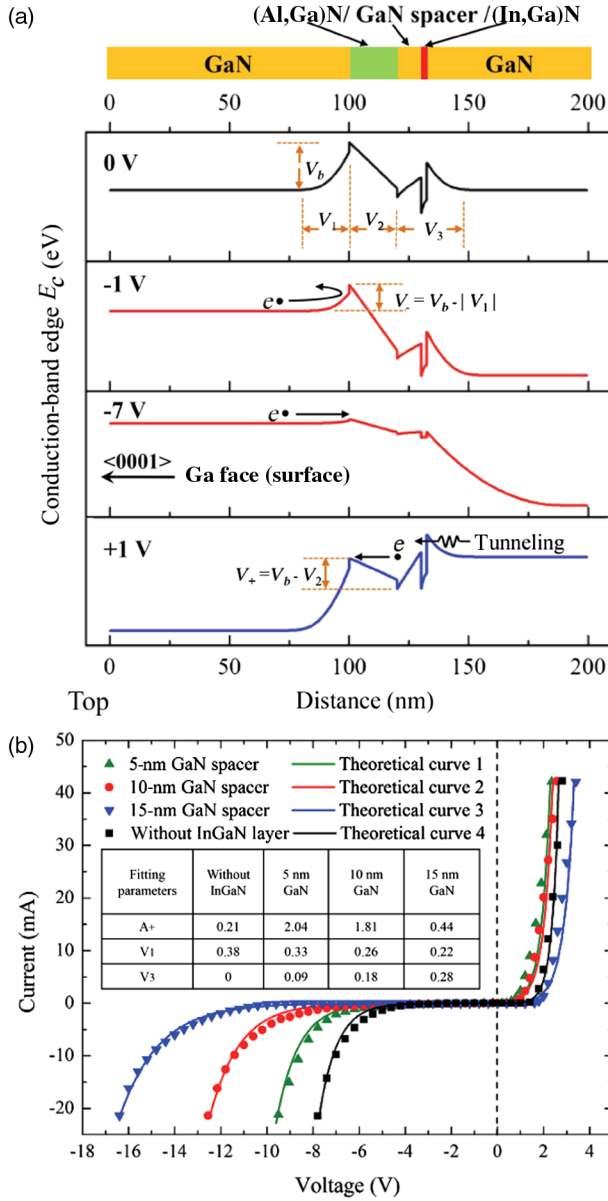


FIG. 4. (a) Conduction-band diagrams of sample with the 10-nm GaN spacer and 2.5-nm $\text{In}_{0.2}\text{Ga}_{0.8}\text{N}$ layer under different applied voltages $V_a = V_1 + V_2 + V_3$ [27]. $V_{1,2}$ are the voltage drops on the GaN depletion region and (Al,Ga)N barrier, and V_3 the voltage drop on the (In,Ga)N-related region. V_b is the height of the (Al,Ga)N barrier at zero bias. (b) Comparison of experimental measurements and theoretical I - V curves. Inset: The best-fitted parameters of A_+ , V_1 , and V_3 for samples with different GaN spacer thicknesses; V_1 and V_3 are in units of V_a .

which is about $2 \times 10^{18} \text{ cm}^{-3}$, and h_{\pm} are ideality factors [43].

For convenience, we define $V_1 = \alpha V_a$, $V_2 = (z - \alpha)V_a$, and $V_3 = (1 - z)V_a$ where z and α characterize the distribution of applied voltage V_a . By setting $A_+ = qn_+ \sqrt{kT/2\pi m^*}$ and $A_- = qn_- \sqrt{kT/2\pi m^*}$, the current can be written as

$$I = A_+ \exp\left[-\frac{qV_b - q(z - \alpha)V_a}{h_+ kT}\right] - A_- \exp\left(-\frac{qV_b + q\alpha V_a}{h_- kT}\right). \quad (3)$$

Here, V_b (approximately 0.68 eV) is derived via the electron-energy band structure. A_+ is proportional to the electron density in the electron accumulation region, and $A_- \sim 9.46 \times 10^{-3} \text{ mA}$, which is determined by the electron density in n -GaN. In Table II, we show the best-fitted parameters of the I - V relationships.

For the GaN/ $\text{Al}_x\text{Ga}_{1-x}\text{N}$ /GaN DHs without the (In,Ga)N inserting layer, due to the giant spontaneous and piezoelectric polarization fields in the (Al,Ga)N barrier, the energy bands of the (Al,Ga)N barrier become sharply sloped. As a result, the voltage drops on the (Al,Ga)N barrier and the electron depletion region are different. This is verified in Table II, where $z = 1$ and $V_1 : V_2 = \alpha : (1 - \alpha) = 38 : 62$. In this case, while the (Al,Ga)N barrier is compensated, a slightly larger reverse bias is required to overcome the barrier of the electron depletion region [see Fig. 1(b)], leading to weak rectification effects. Here, the ideality factor h_+ (h_-) is anomalously large ($\gg 2$), which may be contributed by the triangular barrier [43] induced by the polarization fields in the (Al,Ga)N barrier.

We now discuss the situation with the (In,Ga)N quantum-well layer inserted into the DHs. For the reverse bias, the polarization field of the (In,Ga)N layer is offset by the opposite applied field. This offset weakens the slant of the GaN spacer, with a relatively high voltage drop $V_3 = (1 - z)V_a$ on the (In,Ga)N-related region. The voltage drop on the electron depletion region $|V_1| = \alpha|V_a|$ reduces. From Eq. (3), to turn on the device, a higher reverse threshold voltage ($V_a \sim -7 \text{ V}$) is needed; see Fig. 4(a). In Fig. 4(b), we show that the theoretical curves agree well with the experiment measurements. As the thickness of the GaN spacer increases, the reverse voltage drop V_3 on the (In,Ga)N-related region enlarges, and the reverse threshold voltage considerably improves.

Under forward bias, the piezoelectric and spontaneous polarization fields in the (Al,Ga)N barrier are opposite from the external field and, hence, balanced, which lowers the height of the (Al,Ga)N barrier to $V_+ = V_b - V_2$. On the

TABLE II. Best-fitted parameters for the GaN/ $\text{Al}_{0.15}\text{Ga}_{0.85}\text{N}$ /GaN spacer/ $\text{In}_{0.2}\text{Ga}_{0.8}\text{N}$ /GaN samples with and without the (In,Ga)N quantum well.

Fitting parameters	A_+ (mA)	α	z	h_+ (h_-)
Without (In,Ga)N layer	0.21	0.38	1	7 (11.5)
5-nm GaN spacer	2.04	0.33	0.91	8.4 (12.2)
10-nm GaN spacer	1.81	0.26	0.82	8.4 (13)
15-nm GaN spacer	0.44	0.22	0.72	8.4 (14)

other hand, the insertion of the (In,Ga)N quantum-well layer induces the enhancement of the electron concentration in the electron accumulation region with $A_+ \gg A_-$. In this case, the forward current of Eq. (3) is mainly determined by A_+ . For example, for the sample with the 10-nm GaN spacers, in contrast to the sample without the (In,Ga)N layer, A_+ (approximately 1.81 mA) is significantly enhanced [Fig. 4(b)] due to the modulated energy bands of the triangular potential well [Fig. 2(a)]. This enhancement of parameter A_+ can result in the lower forward threshold voltage (+0.9 V). In Table II, the increasing thickness of the GaN spacer leads to the reduction of the parameter A_+ in accordance with the modulated energy bands [Fig. 2(b)]. This reduction of parameter A_+ results in the slight increase of the forward threshold voltage.

In this model, we show that the typical fitted A_+ is at the scale of milliamperes, as shown in Table II. From these data, we can derive the electron-gas density n_+ is about 10^{20} cm^{-3} , which is comparable with the normal two-dimensional electron gas in the triangular potential well of the (Al, Ga)N/GaN interface [3]. We see that the fitting of A_+ agrees well with the normal two-dimensional electron gas.

V. DISCUSSION AND CONCLUSION

Such rectification effects can be further tested by inserting two (In,Ga)N quantum wells into the double heterostructures or thickening the (In,Ga)N quantum-well width. In both cases, the reverse threshold voltages are significantly raised owing to larger voltage drops on the (In,Ga)N-related region (Fig. 5). Simultaneously, the forward turn-on voltages are elevated moderately, since

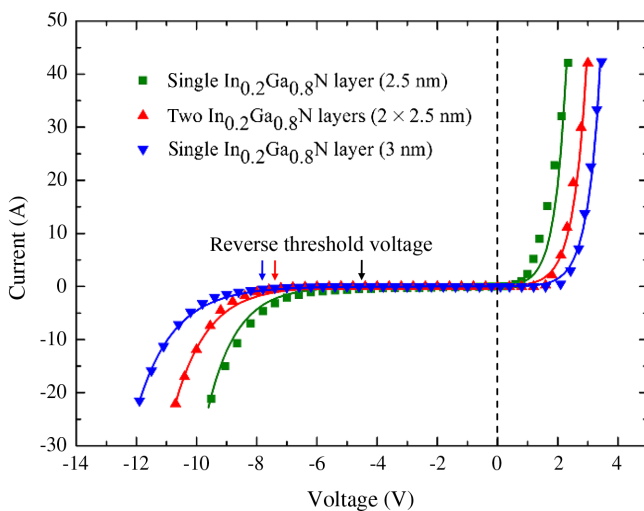


FIG. 5. Measured I - V relationships of the samples with a single thickened (In,Ga)N layer and two (In,Ga)N inserting layers that are separated by a 5-nm GaN spacer. The solid lines are the theoretical curves. Compared to the sample with a single thin (In, Ga)N layer, the reverse threshold voltages are significantly raised, and the forward turn-on voltages are elevated moderately.

the enhanced (In, Ga)N/GaN interface barrier weakens the electron tunneling through them. In addition, here we note that the dislocation density of the samples is at the scale of 10^8 cm^{-2} via counting the etching pits density from the atomic-force-microscope image. The etching of the sample is carried out in the mixture of H_2SO_4 and H_3PO_4 at 170°C for 10 min. The leakage current induced by the dislocations is on the scale of 10^{-3} – 10^{-2} mA under about -10V [44], which is much smaller than the current (0.5 mA) under forward or reverse threshold voltage. Therefore, the threading dislocations make no difference to the measurements of the current-voltage characteristics. Furthermore, the samples are measured as diode chips using a Keithley 4200-SCS to obtain current-voltage relationships, and the scanning speed is 30 ms per point, i.e., about 300 Hz.

In summary, we achieve excellent *p-n* junction rectifications with pure *n*-type (Al,In)GaN structures. Such *p-n* junction characteristics pave the way for GaN-based electronic devices, which avoid the problems of *p*-type GaN. This method can be extended to other important semiconductor materials with giant polarization such as the ZnO material family, offering a scheme for the applications of microelectronics.

ACKNOWLEDGMENTS

We acknowledge support from National Natural Science Foundation of China (Grants No. 11574362, No. 61210014, No. 11374340, and No. 11474205) and the Innovative Clean-Energy Research and Application Program of Beijing Municipal Science and Technology Commission (Grant No. Z151100003515001). We also thank the Laboratory of Microfabrication, Institute of Physics, CAS for the fabrication of devices.

APPENDIX: EXPERIMENTAL AND IMPLEMENTATION DETAILS

1. Material epitaxy

The GaN-based samples are grown in the MOCVD system with a planetary reactor chamber. The precursors are trimethylaluminum, silicohydride, trimethylgallium, triethylgallium, trimethylindium, and ammonia. GaN/(Al, Ga)N/GaN DHs are prepared on *c*-plane sapphire substrates annealed at 1050°C in H_2 , and 25-nm-thick GaN is grown as a nucleation layer at 550°C . Then, the temperature is ramped to 1050°C for annealing and deposition of $3\text{-}\mu\text{m}$ *n*-type GaN:Si ($2 \times 10^{18} \text{ cm}^{-3}$) and 5-nm UID GaN, which are followed by (Al,Ga)N barrier layers and a 100-nm Si-doped GaN layer ($2 \times 10^{18} \text{ cm}^{-3}$). For the samples with (In,Ga)N quantum wells, the (In,Ga)N inserting layers are deposited at 750°C in the full N_2 atmosphere, followed by the UID GaN spacer at the same temperature. The desired indium fraction and thickness are obtained by controlling the growth temperature and time of the (In,Ga)N layer. The compositions of the (In,Ga)N layer

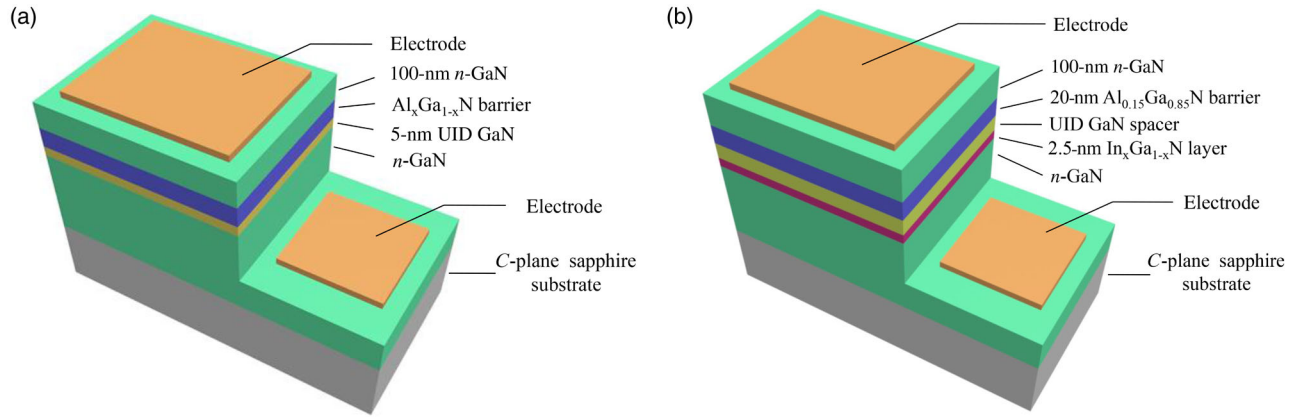


FIG. 6. (a),(b) Schematic structures of the GaN/ $\text{Al}_x\text{Ga}_{1-x}\text{N}$ /GaN DHs and GaN/ $\text{Al}_{0.15}\text{Ga}_{0.85}\text{N}$ /GaN spacer/ $\text{In}_{0.2}\text{Ga}_{0.8}\text{N}$ /GaN samples.

and (Al,Ga)N layer are characterized by high-resolution x-ray diffraction.

2. Device fabrication and characterization

We use an inductively-coupled-plasma-reactive-ion-etching system to achieve mesa isolation and expose the n -GaN buffer. The mesa area is $5000 \mu\text{m}^2$. The electrodes of Cr/Ti/Al (20/20/300 nm) are deposited in sequence by electron-beam evaporation. The samples are measured as diode chips using a Keithley 4200-SCS to obtain current-voltage relationships. The schematic structures of the GaN/ $\text{Al}_x\text{Ga}_{1-x}\text{N}$ /GaN DHs and GaN/ $\text{Al}_{0.15}\text{Ga}_{0.85}\text{N}$ /GaN spacer/ $\text{In}_{0.2}\text{Ga}_{0.8}\text{N}$ /GaN samples are shown in Fig. 6.

For the contact characteristics between the electrodes and n -GaN, the current-voltage measurement is performed on the two bottom electrodes. The linear correlation shows the Ohmic nature of the contact between electrode (Cr/Ti/Al) and the bottom n -GaN, as shown in the inset of Fig. 1(a). However, this method cannot be applied directly to the top contact between the electrodes and the top n -GaN, since the current paths contain not only the surface n -GaN but also the inserting layers. To demonstrate that the contact between the Cr/Ti/Al electrode and top n -GaN is Ohmic, we increase the thickness of the top n -GaN from 100 to 500 nm. As the top n -GaN is thick enough (500 nm), the inserting structure cannot deplete the electrons of the top n -GaN, and the contact is Ohmic. We find that the I - V characteristic of the top contacts with 100- or 500-nm GaN does not significantly change. This indicates the Ohmic nature of the top contact between the Cr/Ti/Al electrode and 100-nm n -GaN.

3. Simulations of the energy-band diagrams

The energy-band diagrams of the GaN/(Al, Ga)N/GaN DHs and samples with the (In,Ga)N layer in the text are obtained through simulation using the ATLAS simulation tool from Silvaco.

- [1] S. J. Pearton and F. Ren, GaN electronics, *Adv. Mater.* **12**, 1571 (2000).
- [2] F. Bernardini, V. Fiorentini, and D. Vanderbilt, Spontaneous polarization and piezoelectric constants of III-V nitrides, *Phys. Rev. B* **56**, R10024 (1997).
- [3] O. Ambacher, J. Smart, J. R. Shealy, N. G. Weimann, K. Chu, M. Murphy, W. J. Schaff, L. F. Eastman, R. Dimitrov, L. Wittmer, M. Stutzmann, W. Rieger, and J. Hilsenbeck, Two-dimensional electron gases induced by spontaneous and piezoelectric polarization charges in N- and Ga-face AlGaIn/GaN heterostructures, *J. Appl. Phys.* **85**, 3222 (1999).
- [4] J. Simon, Z. Zhang, K. Goodman, H. Xing, T. Kosel, P. Fay, and D. Jena, Polarization-Induced Zener Tunnel Junctions in Wide-Band-Gap Heterostructures, *Phys. Rev. Lett.* **103**, 026801 (2009).
- [5] O. Ambacher, B. Foutz, J. Smart, J. R. Shealy, N. G. Weimann, K. Chu, M. Murphy, A. J. Sierakowski, W. J. Schaff, L. F. Eastman, R. Dimitrov, A. Mitchell, and M. Stutzmann, Two dimensional electron gases induced by spontaneous and piezoelectric polarization in undoped and doped AlGaIn/GaN heterostructures, *J. Appl. Phys.* **87**, 334 (2000).
- [6] I. Vurgaftman, J. R. Meyer, and L. R. Ram-Mohan, Band parameters for III-V compound semiconductors and their alloys, *J. Appl. Phys.* **89**, 5815 (2001).
- [7] R. Li, S. J. Cai, L. Wong, Y. Chen, K. L. Wang, R. P. Smith, S. C. Martin, K. S. Boutros, and J. M. Redwing, An $\text{Al}_{0.3}\text{Ga}_{0.7}\text{N}$ /GaN undoped channel heterostructure field effect transistor with F_{max} of 107 GHz, *IEEE Electron Device Lett.* **20**, 323 (1999).
- [8] F. Ren and J. C. Zolper, *Wide Energy Bandgap Electronic Devices* (World Scientific, London, 2003).
- [9] S. K. O'Leary, B. E. Foutz, M. S. Shur, and L. F. Eastman, Steady-state and transient electron transport within the III-V nitride semiconductors, GaN, AlN, and InN: A review, *J. Mater. Sci.* **17**, 87 (2006).
- [10] J. M. Redwing, M. A. Tischler, J. S. Flynn, S. Elhamri, M. Ahoujja, R. S. Newrock, and W. C. Mitchell, Two-dimensional electron gas properties of AlGaIn/GaN

- heterostructures grown on 6H-SiC and sapphire substrates, *Appl. Phys. Lett.* **69**, 963 (1996).
- [11] S. Huang, X. Y. Liu, J. H. Zhang, K. Wei, G. G. Liu, X. H. Wang, Y. K. Zheng, H. G. Liu, Z. Jin, C. Zhao, C. Liu, S. H. Liu, S. Yang, J. C. Zhang, Y. Hao, and K. J. Chen, High RF performance enhancement-mode Al₂O₃/AlGa_xN/GaN MIS-HEMTs fabricated with high-temperature gate-recess technique, *IEEE Electron Device Lett.* **36**, 754 (2015).
- [12] M. A. Khan, A. Bhattarai, J. N. Kuznia, and D. T. Olson, High electron mobility transistor based on a GaN-Al_xGa_{1-x}N heterojunction, *Appl. Phys. Lett.* **63**, 1214 (1993).
- [13] A. T. Schremer, J. A. Smart, Y. Wang, O. Ambacher, N. C. MacDonald, and J. R. Shealy, High electron mobility AlGa_xN/GaN heterostructure on (111)Si, *Appl. Phys. Lett.* **76**, 736 (2000).
- [14] Y. Xiang, X. J. Chen, C. Ji, X. L. Yang, F. J. Xu, Z. J. Yang, X. N. Kang, B. Shen, G. Y. Zhang, and T. J. Yu, Temperature-dependent polarization characteristics in Al_{0.25}Ga_{0.75}N/AlN/GaN heterostructure, *Appl. Phys. Lett.* **108**, 063503 (2016).
- [15] R. Oberhuber, G. Zandler, and P. Vogl, Mobility of two-dimensional electrons in AlGa_xN/GaN modulation-doped field-effect transistors, *Appl. Phys. Lett.* **73**, 818 (1998).
- [16] S. Huang, K. Wei, G. G. Liu, Y. K. Zheng, X. H. Wang, L. Pang, X. Kong, X. Y. Liu, Z. K. Tang, S. Yang, Q. M. Jiang, and K. J. Chen, High-fMAX high Johnson's figure-of-merit 0.2 μm gate AlGa_xN/GaN HEMTs on silicon substrate with AlN/SiN_x passivation, *IEEE Electron Device Lett.* **35**, 315 (2014).
- [17] S. Nakamura, N. Iwasa, M. Senoh, and T. Mukai, Hole compensation mechanism of p-type GaN films, *Jpn. J. Appl. Phys.* **31**, 1258 (1992).
- [18] U. Kaufmann, P. Schlotter, H. Obloh, K. Köhler, and M. Maier, Hole conductivity and compensation in epitaxial GaN:Mg layers, *Phys. Rev. B* **62**, 10867 (2000).
- [19] D. C. Look, D. C. Reynolds, J. W. Hemsky, J. R. Sizelove, R. L. Jones, and R. J. Molnar, Defect Donor and Acceptor in GaN, *Phys. Rev. Lett.* **79**, 2273 (1997).
- [20] D. Lee, B. Mitchell, Y. Fujiwara, and V. Dierolf, Thermodynamics and Kinetics of Three Mg-H-V_N Complexes in Mg:GaN from Combined First-Principles Calculation and Experiment, *Phys. Rev. Lett.* **112**, 205501 (2014).
- [21] H. Amano, M. Kito, K. Hiramatsu, and I. Akasaki, P-type conduction in Mg-doped GaN treated with low-energy electron beam irradiation (LEEBI), *Jpn. J. Appl. Phys.* **28**, L2112 (1989).
- [22] S. Nakamura, T. Mukai, M. Senoh, and N. Iwasa, Thermal annealing effects on p-type Mg-doped GaN films, *Jpn. J. Appl. Phys.* **31**, L139 (1992).
- [23] J. Simon, V. Protasenko, C. X. Lian, H. L. Xing, and D. Jena, Polarization-induced hole doping in wide-band-gap uniaxial semiconductor heterostructures, *Science* **327**, 60 (2010).
- [24] J. K. Sheu and G. C. Chi, The doping process and dopant characteristics of GaN, *J. Phys. Condens. Matter* **14**, R657 (2002).
- [25] A. Chandra and L. F. Eastman, Rectification at n-n GaAs: (Ga,Al)As heterojunctions, *Electron. Lett.* **15**, 90 (1979).
- [26] S. R. Forrest and O. K. Kim, An n-In_{0.53}Ga_{0.47}As/n-InP rectifier, *J. Appl. Phys.* **52**, 5838 (1981).
- [27] The energy-band diagrams of the GaN/(Al, Ga)N/GaN DHs and samples with an (In,Ga)N layer are obtained through simulation using the ATLAS simulation tool from Silvaco.
- [28] I. Hase, H. Kawai, K. Kaneko, and N. Watanabe, Electron transport through the MOCVD grown GaAs/AlGaAs/GaAs heterojunction barrier, *Electron. Lett.* **20**, 491 (1984).
- [29] I. Akasaki, Blue light: A fascinating journey (Nobel lecture), *Angew. Chem., Int. Ed. Engl.* **54**, 7750 (2015).
- [30] F. A. Ponce and D. P. Bour, Nitride-based semiconductors for blue and green light-emitting devices, *Nature (London)* **386**, 351 (1997).
- [31] P. Waltereit, O. Brandt, A. Trampert, H. T. Grahn, J. Menniger, M. Ramsteiner, M. Reiche, and K. H. Ploog, Nitride semiconductors free of electrostatic fields for efficient white light-emitting diodes, *Nature (London)* **406**, 865 (2000).
- [32] S. Nakamura, M. Senoh, S. Nagahama, N. Iwasa, T. Yamada, T. Matsushita, H. Kiyoku, and Y. Sugimoto, InGa_xN-based multi-quantum-well-structure laser diodes, *Jpn. J. Appl. Phys.* **35**, L74 (1996).
- [33] S. Nakamura, S. Pearton, and G. Fasol, *The Blue Laser Diode: The Complete Story* (Springer-Verlag, New York, 2000).
- [34] O. Jani, I. Ferguson, C. Honsberg, and S. Kurtz, Design and characterization of GaN/InGa_xN solar cells, *Appl. Phys. Lett.* **91**, 132117 (2007).
- [35] C. J. Neufeld, N. G. Toledo, S. C. Cruz, M. Iza, S. P. Denbaars, and U. K. Mishra, High quantum efficiency InGa_xN/GaN solar cells with 2.95 eV band gap, *Appl. Phys. Lett.* **93**, 143502 (2008).
- [36] A. Link, T. Graf, R. Dimitrov, O. Ambacher, M. Stutzmann, Y. Smorchkova, U. Mishra, and J. Speck, Transport properties of two-dimensional electron gases induced by spontaneous and piezoelectric polarisation in AlGa_xN/GaN heterostructures, *Phys. Status Solidi (b)* **228**, 603 (2001).
- [37] Q. Peng, G. Yu, C. Zhang, Y. Yang, and A. J. Heeger, Polymer light-emitting electrochemical cells, *Science* **269**, 1086 (1995).
- [38] E. A. Gulians, C. Ji, Young J. Song, and W. A. Anderson, A 0.5 μm thick polycrystalline silicon Schottky diode with rectification ratio of 10⁶, *Appl. Phys. Lett.* **80**, 1474 (2002).
- [39] S. Karan and B. Mallik, Nanostructured organic-inorganic photodiodes with high rectification ratio, *Nanotechnology* **19**, 495202 (2008).
- [40] S. M. Sze and K. K. Ng, *Physics of Semiconductor Devices* (Wiley, Hoboken, NJ, 2007).
- [41] S. S. Perlman and D. L. Feucht, p-n heterojunctions, *Solid State Electron.* **7**, 911 (1964).
- [42] R. J. Anderson, Experiments on Ge-GaAs heterojunctions, *Solid State Electron.* **5**, 341 (1962).
- [43] D. Zhu, J. Xu, A. N. Noemaun, J. K. Kim, E. F. Schubert, M. H. Crawford, and D. D. Koleske, The origin of the high diode-ideality factors in GaInN/GaN multiple quantum well light-emitting diodes, *Appl. Phys. Lett.* **94**, 081113 (2009).
- [44] D. S. Li, H. Chen, H. B. Yu, H. Q. Jia, Q. Huang, and J. M. Zhou, Dependence of leakage current on dislocations in GaN-based light-emitting diodes, *J. Appl. Phys.* **96**, 1111 (2004).